Journal of Power Sources 260 (2014) 72–76

Contents lists available at ScienceDirect

Journal of Power Sources

journal homepage: www.elsevier.com/locate/jpowsour

Short communication

The new electrochemical reaction mechanism of Na/FeS_2 cell at ambient temperature

Zulipiya Shadike [a,1], Yong-Ning Zhou [b,1], Fei Ding [c], Lin Sang [c], Kyung-Wan Nam [b], Xiao-Qing Yang [b], Zheng-Wen Fu [a,*]

[a] Shanghai Key Laboratory of Molecular Catalysts and Innovative Materials, Department of Chemistry & Laser Chemistry Institute, Fudan University, Shanghai 200433, PR China
[b] Chemistry Department, Brookhaven National Laboratory, Upton, NY 11973, USA
[c] National Key Laboratory of Science and Technology on Power Sources, Tianjin Institute of Power Sources, Tianjin 300384, PR China

HIGHLIGHTS

- We have fabricated the FeS_2 particle by hydrothermal process.
- We have examined the electrochemical behaviors of FeS_2 with sodium.
- We have clarified the charge reaction mechanism of Na/FeS_2 cell for the first time.

ARTICLE INFO

Article history:
Received 1 January 2014
Received in revised form
19 February 2014
Accepted 4 March 2014
Available online 14 March 2014

Keywords:
FeS_2
Sodium ion battery
Charge reaction mechanism
Hydrothermal synthesis

ABSTRACT

FeS_2 synthesized by hydrothermal method was used for sodium batteries for the first time. A large initial discharge capacity of 771 mAh g^{-1} and a high reversible capacity of 521 mAh g^{-1} were obtained. The reaction mechanism of electrochemical de-sodiation (charge) was investigated after the initial discharge. Our results have demonstrated that the composition and structure of electrode after the charging to 3.0 V could not recover its original state of FeS_2 and a new phase of $NaFeS_2$ was revealed. This should be responsible to the large irreversible capacity in the first cycle and the high discharge and charge plateaus after the initial cycle.

1. Introduction

Iron disulfide is an interesting material for electrochemical energy storage systems such as lithium and sodium batteries due to its low cost and environmental friendly nature, as well as its potential to offer high capacity and energy density when used as an advanced energy storage material. Cathode materials based on FeS_2 for sodium ion secondary battery (SIB) at room temperature have been reported in the literature [1–4]. Kim et al. [1] first reported the rechargeable Na/FeS_2 battery operated at room temperature with a high discharge capacity of 630 mAh g^{-1}. The possible discharge reactions of FeS_2 with sodium resulted in various sodium polysulfides such as Na_2S_2 or Na_2S and metallic Fe was proposed from the Na–S binary phase diagram [2]. The discharge capacities of FeS_2 powder were found to be dependent on its particle sizes associated with the synthesis conditions [2,3]. Kitajou et al. studied the reaction mechanism of FeS_2 with Na during electrochemical discharge using synchrotron-based X-ray absorption near edge spectroscopy (XANES) and other spectroscopic techniques, and revealed the formation of Na_2S and metallic Fe as discharged products [4]. All of these works provided important information about the electrochemical properties of sodium-FeS_2 cell and the possibility of using it as energy storage material for the application and development of SIB. Consequently, the legitimate question remains what the charge reaction mechanism of metallic Fe with Na_2S formed after the initial discharge process is? For instance, whether FeS_2 could be reversible produced by the electrochemical reaction of Na_2S with metallic Fe during the charge process? Apparently, the electrochemical charge reaction mechanism of FeS_2 with Na still need to be further investigated.

* Corresponding author. Tel.: +86 21 65642522; fax: +86 21 65102777.
E-mail addresses: xyang@bnl.gov (X.-Q. Yang), zwfu@fudan.edu.cn (Z.-W. Fu).
[1] Zulipiya Shadike and Yong-Ning Zhou contributed equally to this work.

http://dx.doi.org/10.1016/j.jpowsour.2014.03.011
0378-7753/

Here, we will report the hydrothermal synthesis of FeS_2 as cathode material for sodium batteries for the first time. The physical and electrochemical properties of FeS_2 are examined by scanning electron Microscopy (SEM), X-ray diffraction (XRD), transmission electron microscopy (TEM), X-ray absorption spectroscopy (XAS), cyclic voltammogram(CV) and galvanostatic cycling measurements. The reaction mechanism of FeS_2 with sodium during electrochemical recharge process will be discussed in detail for clarifying the intrinsic properties of FeS_2 electrode.

2. Experimental

FeS_2 particle was synthesized by a simply hydrothermal method [5]. 3.08 mmol of sulfur powder was dissolved in 2.2 mL of Ethylenediamine under constant stirring. To witch 2.4 g polyvinylpyrrolidone dissolved in17.0 mL deionized (DI) water and 1.54 mmol of $FeCl_2 \cdot 4H_2O$ were added in sequence under vigorous string. The mixture was sealed in Teflon-lined stainless steel autoclave and put into muffle heated oven at 200 °C for 24 h.The resulting product was collected by centrifugation, washed with DI water and absolute ethanol for several times and dried at 70 °C under vacuum overnight.

The as-synthesized powders were characterized by X-ray diffraction (XRD, Bruker D8 ADVANCE) with a monochromatized source of Cu Kα1 radiation (λ = 0.1540 nm) at 1.6 kW output power. Scanning electron microscopy (SEM, Cambridge S-360) was employed to study the morphology and particle size distribution of the products. TEM and SAED measurements were carried out by 200 kV side entry JEOL 2010 TEM. The *in situ* XRD spectra were collected at beamline X14A of National Synchrotron Light Source (NSLS) at Brookhaven National Laboratory using a linear position sensitive silicon detector. The wavelength used was 0.7747 Å. XAS was performed at beamline X19A of NSLS. Fe K-edge XAS was collected in transmission mode, while S K-edge XAS was in fluorescence mode. The XAS data was processed using Athena [6].

For the electrochemical measurements, the working electrode consisted of active material (FeS_2 sample, 70 wt. %), electrical conductor (acetylene black, 20 wt. %), and binder (PVDF, 10 wt. %) was coated on aluminum foil current collector. The cells were constructed by using FeS_2 cathode as a working electrode and two sodium sheets as counter electrode and reference electrode, respectively. The cells were assembled in an argon-filled glove box using 1 M $NaClO_4$ (Aldrich) solution in a nonaqueous ethylene carbonate (EC)–Propylene carbonate (PC) (1:1 in volume) mixed solvents as the electrolyte. Galvanostatic charge–discharge measurements were carried out at room temperature with a Land CT 2001A battery test system. The cells were cycled between 0.9 and 3.0 V vs. Na^+/Na. Cyclic voltammogram (CV) tests were performed on a CHI660A electrochemical working station (CHI instruments).

3. Result and discussion

Fig. 1(a) shows the SEM images of FeS_2 particles synthesized by hydrothermal process. As can be seen, the FeS_2 particles show budlike microspheres as secondary particles with diameters of about 4 μm. In addition, these microparticles composed of smaller particles contacting each other randomly. The sizes of these primary particles are in the range of 0.7–1 μm. Fig. 1(b) presents the XRD pattern of the FeS_2 powder. It clearly shows that all the diffraction peaks of the powder matched well with the cubic pyrite FeS_2 (JCPDS No.42-1340) and no peaks representing impurity phase were observed.

Fig. 1(d) shows the first three cyclic voltammograms of FeS_2 electrode between 0.9 and 3.0 V measured at a scan rate of 0.1 mV s^{-1}. The first reduction process shows one distinguishable peak at about 1.1 V, which could be attributed to the decomposition of FeS_2. After the initial cycle, this peak was no longer

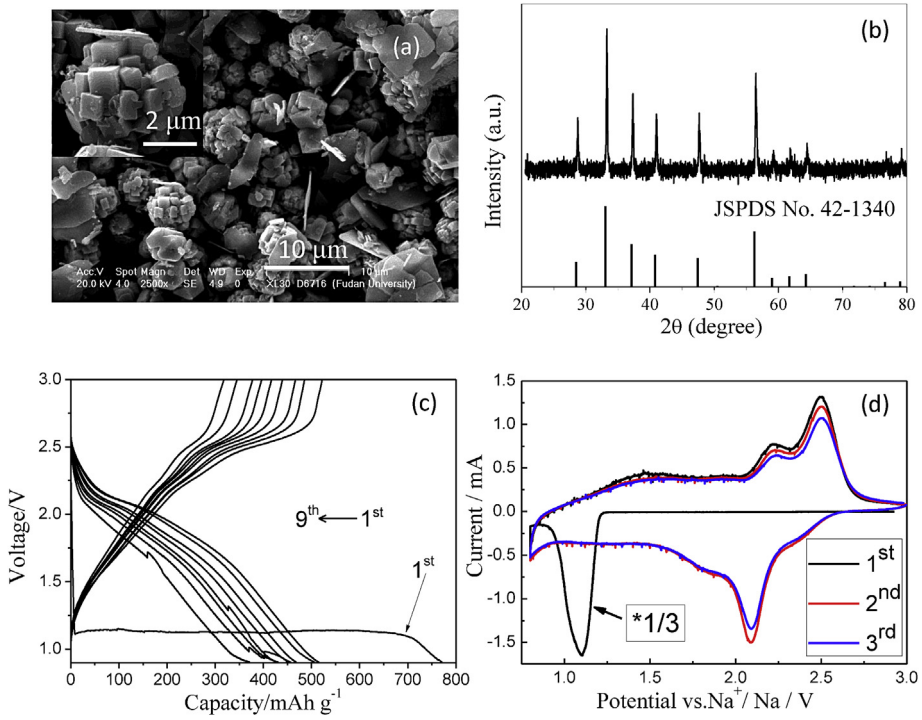

Fig. 1. (a) the SEM images and (b) XRD pattern of FeS_2 hierarchical particles synthesized by hydrothermal process; (c) galvanostatic cycling profiles of the FeS_2/Na cells cycled between 0.9 and 3.0 V at the current densities of 40 mA g^{-1}; (d) the first three cyclic voltammograms for the FeS_2 electrode at a voltage sweep rate of 0.1 mA s^{-1}.

present in subsequent cycles. In contrast, two different peaks at 1.8 and 2.1 V, which are likely to be the counterparts of two anodic peaks at 2.2 and 2.5 V were observed. They may be related to multi-steps reaction mechanism. The summation of the integrated area of these two peaks is less than the first one, indicating large irreversibility of this reaction. This is in a good agreement with the irreversible capacity loss between the first two cycles observed in galvanostatic curves. In the subsequent cycles, these two couple of peaks for each cycle were almost overlapped, indicating that highly reversible reactions took place during the subsequent cycles. The shapes of oxidation peaks are well maintained in all subsequent cycles.

The galvanostatic cycling was performed to examine the electrochemical behavior of FeS_2 reacting with sodium, and its voltage–capacity profiles are presented in Fig. 1(c). The initial open-circuit voltage of the cell is 2.92 V. The first discharge curve show an abrupt drop in voltage with a long plateau at 1.1 V and a high-specific discharge capacity of 771 mAh g^{-1}. This corresponds to about 4.0 Na per FeS_2. This is similar to the result of FeS_2 prepared by mechanical alloying of natural pyrite [1–3], corresponding to the reaction of FeS_2 and Na into Na_2S and Fe. In the first recharge process, there are two sloping plateaus centered at 2.2 and 2.5 V. These two plateaus recover 67.6% of the initial discharge capacity and yield a total recharge capacity of 521 mAh g^{-1}. In the subsequent cycles, the discharge curves are similar to each other, but utterly different from the initial discharge, implying a change of structure or composition of the electrode through the first charge process. Because the theoretical electromotive force of Na_2S is 1.85 V [7], a considerable value of discharge capacity about 200 mAh g^{-1} between 3.0 and 1.85 V at the second cycles cannot be explained by the formation of Na_2S as described before for the first discharge process. Such a high discharge plateau after the first cycles indicates that the products obtained after the first recharge are not exactly the same as the pristine FeS_2.

In order to investigate the charge reaction mechanism of Na/FeS_2 cell, the synchrotron-based *in situ* XRD technique was employed. The FeS_2 electrode was firstly sodiated in the cell by discharge to 0.9 V at a constant current of 20 μA cm^{-2}, then the *in situ* XRD data was recorded upon recharge. Fig. 2(a) shows the synchrotron-based *in situ* XRD patterns along with the first charge curve. Besides two diffraction peaks at $2\theta = 33.1°$ and 35.6° of the Al foil current collector, no any other diffraction peak of full discharged product is observed. This may be due to the nanosize nature of the Na_2S and Fe formed through the discharge process. When the particle size (and grain size) becomes so small, the Bragg peaks of the crystal sample will be too broad and too weak to be detected by XRD. Interestingly, a new peak emerges at about $2\theta = 31.4°$ when the *x* values reached less than 2.0 in Na_xFeS_2 as shown in red arrow in Fig. 2(a) and a progressive intensity increase of the peak at $2\theta = 31.4°$ is observed during charge to 3.0 V. This peak at $2\theta = 31.4°$ can be indexed to (2 2 1) of $NaFeS_2$ (JCPDS 34-935). It should be noted that this is the only peak can be seen from the sample due to the poor crystallinity after recharge, which normally happens for the electrode based on conversion reactions [8].

X-ray absorption spectroscopy was carried out to determine the variation in valence and local structure around Fe and S in the sodiated and desodiated electrodes. Fig. 2(b) shows the Fe and S K-edge XANES of the FeS_2 electrode after discharge to 0.9 V and recharge to 3.0 V, in comparing with the pristine sample. In the initial state, the Fe K-edge absorption energy at 7118.3 eV and S K-edge absorption energy at 2471.1 eV could be assigned to Fe^{2+} [4,9,10] and S_2^{2-} [11–13] of FeS_2, respectively. After discharging to 0.9 V, both shapes of the Fe and S K-edge XANES spectra were

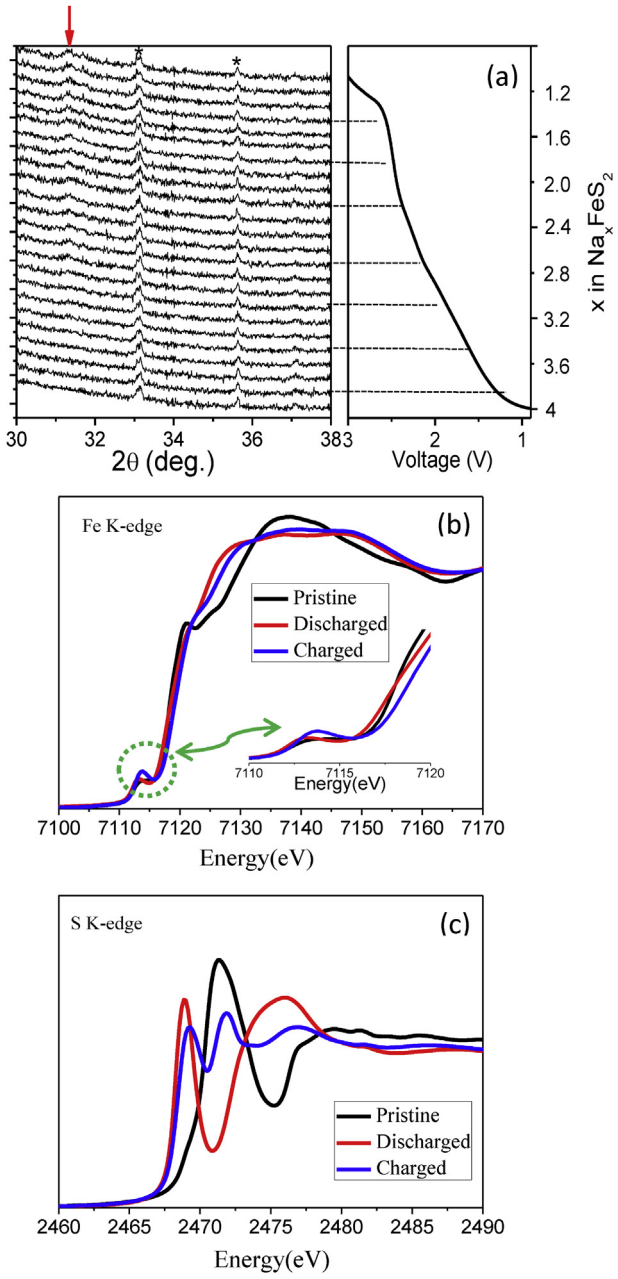

Fig. 2. (a) *In situ* X-ray diffraction patterns collected during the first charge for FeS_2/Na cell. The corresponding voltage-composition profile is given on the right side XRD patterns at a current density of 20 mA g^{-1}; Normalized (b) Fe K-edge XANES spectra (c) S K-edge XANES spectra of the FeS_2 at pristine, charged and discharged states. (For interpretation of the references to color in this figure legend, the reader is referred to the web version of this article).

different from those of the initial state. The main change of the Fe K-edge was that the upper part of the white line shifts to the lower energy, indicating the reduction of Fe during discharge, but the spectra after discharge is still different from that of metal Fe (Fe^0) [4,10]. This result is same as the previous report by Kitajou et al. [4]. It may be due to the incomplete reduction of Fe^{2+} or the local structure difference between the electrochemically formed Fe and reference Fe foil. However, the formation of metallic Fe after discharge will be confirmed by TEM results mentioned below and the XPS results in the literature [4]. The corresponding S K-edge shows a clear shift from 2471.1 to 2468.3 eV, corresponding to the

change from S_2^{2-} to S^{2-} [6,12,13]. When the cell was charged to 3.0 V, the Fe K-edge shifted to the higher energy, but it did not fully recovered to the original state as the pristine sample. In addition, a clear increase of the pre-edge peak intensity was observed, indicating that Fe ion was oxidized resulting in a more empty 3d orbital. The local structure and coordination of Fe in the charged products were quite different from those of the pristine FeS_2. From the S K-edge of the charged sample, it can be seen that the edge position moved back to the original, but some residual feature (peak at 2472 eV) from the discharged products was still there. It implied that the S^{2-} was mostly oxidized back to S_2^{2-} after charge but not fully recovered to the original state for the pristine sample. The remarkable differences of Fe and S K-edge XANES spectra between the desodiated and pristine electrodes suggest that the composition and structure of electrode after charging to 3.0 V could not be fully recovered to its original state of FeS_2, and a new desodiated product is formed as confirmed by XRD data.

To further detect the composition and structure of the sodiated and desodiated electrodes, *ex situ* TEM and SAED measurements were employed. Fig. 3(a) shows the typical TEM image of the FeS_2 after firstly discharging to 0.9 V. However, we could only see some ambiguous stripes because the local product is unstable and these black domains are gradually thawing with further focusing TEM e-beam on the sample. The corresponding SAED pattern shown in Fig. 3(b) consists of several bright rings made up of discrete spots. These discrete diffraction spots could be unambiguously indexed to diffractions of Na_2S phase (JCPDS 65-2995) and Fe (JCPDS 6-696). The result is in good agreement with previous reports using XANES technique [4]. After recharge to 3.0 V, some strips can be seen clearly in the high resolution TEM image (Fig. 3(c)). After measuring the d-space, the lattice plane could be attributed to the (2 2 0) plane of $NaFeS_2$. The SAED pattern in this region is shown in Fig. 3(d). All d-spacings from the SAED spectra can be well indexed to $NaFeS_2$ (JCPDS 34-935) and listed in Table 1, which is totally different from the pyrite structure for the pristine sample. This result is consistent with the results obtained from *in situ* XRD and *ex situ* XAS measurements.

Table 1
d-spacings (Å) derived from SAED analysis of the electrode after the first discharging to 0.9 V and the charging to 3.0 V. JCPDS standards for Na_2S, Fe and $NaFeS_2$ are shown for references.

First discharging to 0.9 V			
Na_2S		Fe	
Fm-3m(65-2995)		Im-3m(6-696)	
T.W.	Reference	T.W.	Reference
3.76	3.77(1 1 1)	2.03	2.02(1 1 0)
3.26	3.26(2 0 0)	1.43	1.43(2 0 0)
2.33	2.31(2 2 0)		
$a = 6.54 \pm 0.06$	$a = 6.54$	$a = 2.87 \pm 0.01$	$a = 2.87$
First charging to 3.0 V			
$NaFeS_2$			
Pa(34-935)			
T.W.	Reference		
3.30	3.33(3 1 0)		
3.30	3.33(1 2 1)		
2.37	2.35(0 2 2)		
2.02	2.01(1 3 -2)		
$a = 10.61 \pm 0.05$	$a = 10.69$		
$b = 9.13 \pm 0.07$	$b = 9.10$		
$c = 5.49 \pm 0.03$	$c = 5.51$		
$\beta = 93.6° \pm 0.09°$	$\beta = 92.1°$		

*TW: This work.

The electrochemical reaction mechanism of FeS_2 with sodium after the initial discharge might be proposed as following

$$Fe + 2Na_2S - (4 - x)e \leftrightarrow (4 - x)Na^+ + Na_xFeS_2 \quad (1)$$

Here, the inserted coefficient x is estimated to be 0.7 from the charge capacity. A nano-sized Na_2S and Fe were formed in the initial discharge process from an irreversible reaction of FeS_2 with sodium. The recharging processes involve two different desodiation reactions at least, since two couples of reduction and oxidation

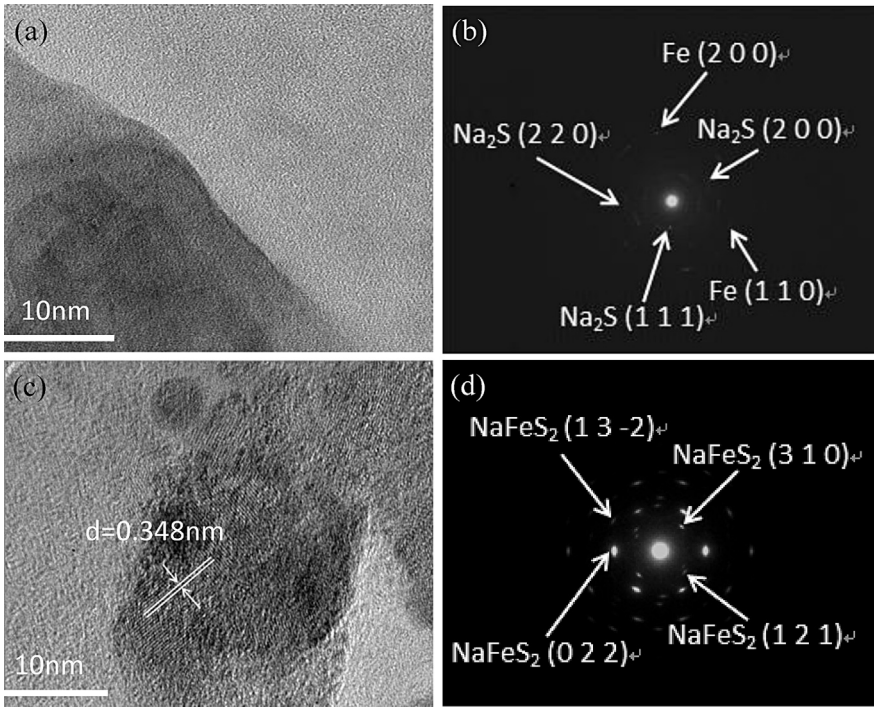

Fig. 3. The *ex situ* TEM images of the FeS_2 electrodes (a) after the first discharging to 0.9 V; (c) after the first charging to 3.0 V and their corresponding SAED patterns (b) and (d).

peaks at 1.8, 2.1 V and 2.2, 2.5 V in CV curves were obtained. They include the intercalation/deintercalation reactions of $NaFeS_2$ and the conversion reactions of nanocrystalline Na_2S and Fe. This reaction mechanism should be responsible for the large irreversible capacity during the first cycle, as well as the high discharge and charge plateaus after the initial cycle.

4. Conclusion

In this study, we found that FeS_2 could not be reversible produced by the electrochemical reaction of Na_2S with metallic Fe during the first recharge process. Instead, a new $NaFeS_2$ phase was formed. The subsequent electrochemical behavior should be attributed to the reversible intercalation/deintercalation reactions of $NaFeS_2$ phase and the conversion reactions of nanocrystalline Na_2S and Fe after the initial discharge. Further detailed investigation on this system is ongoing.

Acknowledgments

This work was financially supported by 973 Program (No. 2011CB933300) of China, Science & Technology Commission of Shanghai Municipality (08DZ2270500 and 11JC1400500), and National Foundation of China (No. B1120132029). The work at Brookhaven National Laboratory was supported by the U.S. Department of Energy, the Assistant Secretary for Energy Efficiency and Renewable Energy, Office of Vehicle Technologies under Contract Number DE-AC02-98CH10886. The authors acknowledge technical supports by the beamline scientists at X14A and X19A at NSLS, BNL.

References

[1] T.B. Kim, J.W. Choi, H.S. Ryu, G.B. Cho, K.W. Kim, J.H. Ahn, K.K. Cho, H.J. Ahn, J. Power Sources 174 (2007) 1275.
[2] T.B. Kim, W.H. Jung, H.S. Ryu, K.W. Kim, J.H. Ahn, K.K. Cho, G.B. Cho, T.H. Nam, I.S. Ahn, H.J. Ahn, J. Alloys Compd. 449 (2008) 304.
[3] X. Liu, S.D. Kang, J.S. Kim, I.S. Ahn, H.J. Ahn, J. Nanosci. Nanotechnol. 12 (2012) 1563.
[4] A. Kitajou, J. Yamaguchi, S. Hara, S. Okada, J. Power Sources 247 (2014) 391.
[5] L. Zhu, B. Richardson, J. Tanumihardja, Q.M. Yu, Cryst. Eng. Comm. 14 (2012) 4188.
[6] M. Newville, J. Synchrotron. Radiat. 8 (2001) 322.
[7] S. Wenzel, H. Metelmann, C. Raib, A.K. Durr, J. Janek, P. Adelhelm, J. Power Sources 243 (2013) 758.
[8] N. Yamakawa, M. Jiang, B. Key, C.P. Grey, J. Am. Chem. Soc. 131 (2009) 10525.
[9] W. Zhang, P.N. Duchesne, Z.L. Gong, S.Q. Wu, L. Ma, Z. Jiang, S. Zhang, P. Zhang, J.X. Mi, Y. Yang, J. Phys. Chem. C. 117 (2013) 11498.
[10] T. Nedoseykina, M.G. Kim, S.A. Park, H.S. Kim, S.B. Kim, J. Cho, Y. Lee, Electrochim. Acta 55 (2010) 8876.
[11] T. Takeuchi, H. Kageyama, K. Nakanishi, Y. Inada, M. Katayama, T. Ohta, H. Senoh, H. Sakaebe, T. Sakai, K. Tatsumi, H. Kobayashi, J. Electrochem. Soc. 159 (2012) A75.
[12] T. Glaser, K. Rose, S.E. Shadle, B. Hedman, K.O. Hodgson, E.I. Solomon, J. Am. Chem. Soc. 123 (2001) 442.
[13] C. Sugiura, S. Muramatsu, Phys. State Sol. B 129 (1985) K157.